The Astrophysical Journal, 942:5 (7pp), 2023 January 1 https://doi.org/10.3847/1538-4357/aca529

On the Presence of Metallofullerenes in Fullerene-rich Circumstellar Envelopes

R. Barzaga[1,2], D. A. García-Hernández[1,2], S. Díaz-Tendero[3,4,5], SeyedAbdolreza Sadjadi[6,7], A. Manchado[1,2,8], and M. Alcami[3,4,9]
[1] Instituto de Astrofísica de Canarias, C/Vía Láctea s/n, E-38205 La Laguna, Spain; rbarzaga@iac.es
[2] Departamento de Astrofísica, Universidad de La Laguna (ULL), E-38206 La Laguna, Spain
[3] Departmento de Química, Módulo 13, Universidad Autónoma de Madrid, E-28049 Madrid, Spain
[4] Institute for Advanced Research in Chemical Science (IAdChem), Universidad Autónoma de Madrid, E-28049 Madrid, Spain
[5] Condensed Matter Physics Center (IFIMAC), Universidad Autónoma de Madrid, E-28049 Madrid, Spain
[6] Research Center for Theoretical and Experimental Physics, Chemistry and Space Sciences, Genius Development and ScienceTech Future Co. Ltd, Hong Kong (SAR), People's Republic of China
[7] Laboratory for Space Research, Faculty of Science, Department of Physics, The University of Hong Kong, Hong Kong (SAR), People's Republic of China
[8] Consejo Superior de Investigaciones Científicas (CSIC), Spain
[9] Instituto Madrileño de Estudios Avanzados en Nanociencia (IMDEA-Nano), Campus de Cantoblanco, Madrid E-28049, Spain
Received 2022 November 14; revised 2022 November 21; accepted 2022 November 21; published 2022 December 28

Abstract

The presence of neutral C_{60} fullerenes in circumstellar environments has been firmly established by astronomical observations as well as laboratory experiments and quantum-chemistry calculations. However, the large variations observed in the C_{60} 17.4 μm/18.9 μm band ratios indicate that either additional emitters should contribute to the astronomical infrared (IR) spectra or unknown physical processes exist besides thermal and UV excitation. Fullerene-based molecules such as metallofullerenes and fullerene-adducts are natural candidate species as potential additional emitters, but no specific specie has been identified to date. Here we report a model based on quantum-chemistry calculations and IR spectra simulation of neutral and charged endo(exo)hedral metallofullerenes, showing that they have a significant contribution to the four strongest IR bands commonly attributed to neutral C_{60}. These simulations may explain the large range of 17.4 μm/18.9 μm band ratios observed in very different fullerene-rich circumstellar environments like those around planetary nebulae and chemically peculiar R Coronae Borealis stars. Our proposed model also reveals that the 17.4 μm/18.9 μm band ratio in the metallofullerenes simulated IR spectra mainly depends on the metal abundances, ionization level, and endo/exoconcentration in the circumstellar envelopes. We conclude that metallofullerenes are potential emitters contributing to the observed IR spectra in fullerene-rich circumstellar envelopes. Our simulated IR spectra indicate also that the James Webb Space Telescope has the potential to confirm or refute the presence of metallofullerenes (or even other fullerene-based species) in circumstellar environments.

Unified Astronomy Thesaurus concepts: Astrochemistry (75); Circumstellar matter (241); Infrared spectroscopy (2285); Planetary nebulae (1249); R Coronae Borealis variable stars (1327)

1. Introduction

The detection of the most common fullerene species (C_{60}) in planetary nebulae (PNe) and diverse astrophysical environments have raised the exciting possibility that other more complex fullerene-based molecules (e.g., metallofullerenes, multishell fullerenes, and fullerene-adducts) might be ubiquitous in space and continue to be serious candidates to explain several astrophysical phenomena like the unidentified infrared bands (UIRs), the UV-bump, and the diffuse interstellar bands (DIBs), among others (see Kwok 2016, for a review). This idea was reinforced in 2015 when the fullerene cation (C_{60}^+) was established as the only DIB carrier known to date (Campbell et al. 2015).

The presence of neutral C_{60} in space is deduced from the detection of its four strongest mid-IR emission bands (those at ~7.0, 8.5, 17.4, and 18.9 μm).[10] The neutral C_{60} mid-infrared (mid-IR) bands have been (mainly) detected in the circumstellar environments of young PNe (e.g., Cami et al. 2010; García-Hernández et al. 2010) but also in other types of circumstellar environments like those around R Coronae Borealis (RCB) stars (García-Hernández et al. 2011).

Recent experimental studies combined with quantum-chemical calculations also demonstrate that fullerenes would react with metal atoms and molecules (e.g., polycyclic aromatic hydrocarbons; PAHs), forming a rich family of fullerene-based molecules such as endo(exo)hedral metallofullerenes and fullerene–PAH adducts (e.g., Dunk et al. 2013). These fullerene derivatives may still be excited by UV photons, emitting through the same infrared (IR) vibrational modes as empty C_{60} cages. For example, laboratory work shows that the strongest mid-IR features of fullerene–PAH adducts are strikingly similar to those from neutral C_{60}, suggesting that fullerene-based molecules may contribute to the four C_{60} mid-IR features observed in fullerene-containing circumstellar environments (Garcia-Hernandez et al. 2013).

In fact, Brieva et al. (2016) recently made a detailed comparison of their laboratory inferred C_{60} emission band strengths with the astrophysical data on fullerene-rich circumstellar environments, showing that the observed strengths

[10] The mid-IR features of the fullerene cation (C_{60}^+) have only been detected in the reflection nebula NGC 7023 (Berné et al. 2013).

cannot be explained in terms of fluorescent or thermal emission alone. They concluded that the C_{60} emission ratios of 17.4 μm/18.9 μm observed imply that they have a contribution of other emitters, or that physical processes other than thermal or UV excitation affect the C_{60} vibrational modes.[11] Here we present a theoretical study based on quantum-chemistry calculations of endo(exo)hedral metallofullerenes (both neutral and charged), showing that they significantly contribute to the four IR bands generally attributed to neutral C_{60} and may explain the large range of the C_{60} 17.4 μm/18.9 μm band ratio observed in very different circumstellar environments like those around PNe and RCB stars. Our simulated IR spectra indicate that the James Webb Space Telescope (JWST) has the potential to confirm or refute the presence of metallofullerenes in circumstellar environments.

2. Computational Details

Quantum-chemical calculations on the molecular geometry and spectroscopic properties of 28 neutral and charged metallofullerenes have been performed in the framework of the density functional theory (DFT). In particular, geometry optimization was carried out at the B3LYP/6-31G(d) level (Ditchfield et al. 1971; Lee et al. 1988; Becke 1993) with the Gaussian 16 code (Frisch et al. 2016; Dennington et al. 2019). Accuracy benchmarking of this level of theory has been previously reported (Robledo et al. 2014; Wang 2017). Spin multiplicity $(2S+1)$ has been considered in the calculations to a maximum of $S=5/2$, according to the metal multiple-charged states. The chemical formulas of these species are $[\text{M-C}_{60}]^{0/+}$ (exohedral) and $[\text{M@C}_{60}]^{0/+}$ (endohedral) where M = Li, K, Na, Ca, Mg, Fe, Ti.[12] All the geometries used have been characterized as local minimum, with non-imaginary frequencies observed. In order to simulate the vibrational spectra of these species the harmonic oscillator approximation was assumed and, subsequently, harmonic frequencies were adjusted applying a double-scaling-factor scheme to account for anharmonicity, vibrorotational couplings, etc. (Zapata Trujillo & McKemmish 2022). This approach guaranteed an error <2% in the calculated frequencies of C_{60}, used as the benchmarking system, with respect to the experiments (Kern et al. 2013). The total mixture spectra of the metallofullerenes were modeled by the simple addition of each IR intensity. In all the spectra, the peak intensity has been simulated by a Gaussian function of FWHM = 5 cm^{-1}, which is similar to the astronomical observations. The procedure used here, which was implemented to simulate the intensity, accounting for the metal atom concentration/abundance, is presented in Appendix. The atomic charges were obtained from electron density partitioning described by the quantum theory of atoms in molecules (QTAIM), employing the AimAll software (Bader 1990; Keith 2019). Total relative energies have been computed with respect to the most stable structure, thus, it is represented with a value of zero.

[11] Brieva et al. (2016) also demonstrate that, in contrast to other C_{60} band ratios (e.g., those involving the 7.0 and 8.5 μm features), the 17.4 μm/18.9 μm band ratio should remain almost constant independently of the C_{60} excitation model assumed (fluorescence or thermal models).

[12] We consider the most abundant and/or well-known metals to be present in the interstellar medium.

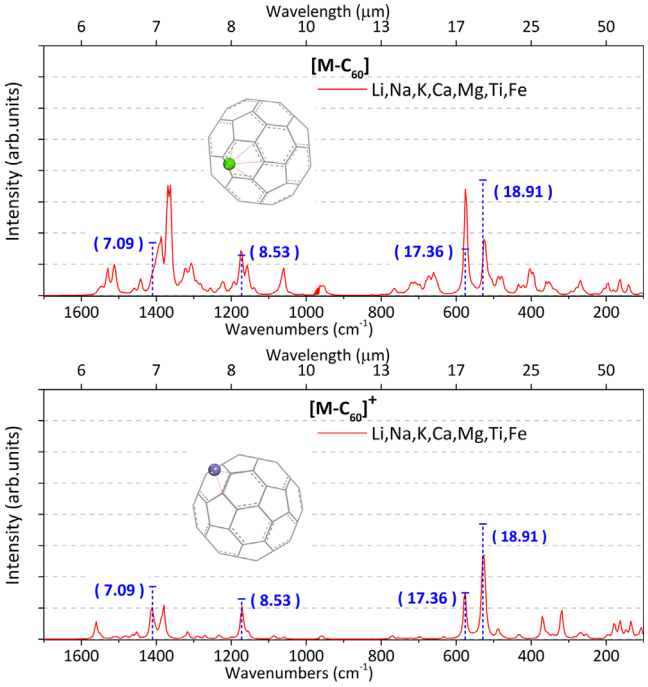

Figure 1. DFT simulated IR (~5–50 μm) spectra of the mixture of metalloexofulerenes. Top panel: seven neutral $[\text{M-C}_{60}]$; bottom panel: seven charged $[\text{M-C}_{60}]^{+}$. The blue dashed lines represent the features of seven pristine C_{60} molecules, whose intensity is described by the height of the lines. The insets display examples of the most common structures obtained.

3. Results and Discussion

The simulated IR (~5–50 μm) spectra in the next two subsections have been constructed from the total mixture spectrum procedure (Section 2). In order to identify the distinctive spectral features of metallofullerenes, Figures 1 and 2 include the four strongest features of C_{60} (Kern et al. 2013; Sadjadi et al. 2022), according to our own calculations (Section 2). The blue dashed lines represent the simulated C_{60} features with a height describing the intensity of the corresponding peak. Note that the intensity of the C_{60} features was scaled equally to the amount of metallofullerenes, i.e., assuming that the same amount of C_{60} molecules and metallofullerenes exist. The total weighted spectrum approach, however, is applied in the third subsection; for further details see Appendix. Further information about the simulated IR spectra for all the metallofullerene species (28) will be publicly available for the astronomical community in a forthcoming paper (R. Barzaga et al.).

3.1. Exofullerenes

Figure 1 shows the mixture of exofullerenes spectra, neutral and charged separately; C_{60} features (shown in blue) are also included for comparison. The positions of the strongest features in both neutral and charged exofullerenes are similar to those of C_{60}.[13] The neutral metalloexofullerenes $[\text{M-C}_{60}]$ exhibit an IR spectrum richer than their charged counterparts, with a broadening and splitting of the IR features, mainly characterized by a modification of their intensity in comparison to C_{60}.

[13] The only exception is the ~7.0 μm feature in the neutral exofullerenes, which is not among the strongest IR features. This feature is certainly present, but blended with the other emission components within the 6–9 μm spectral region.

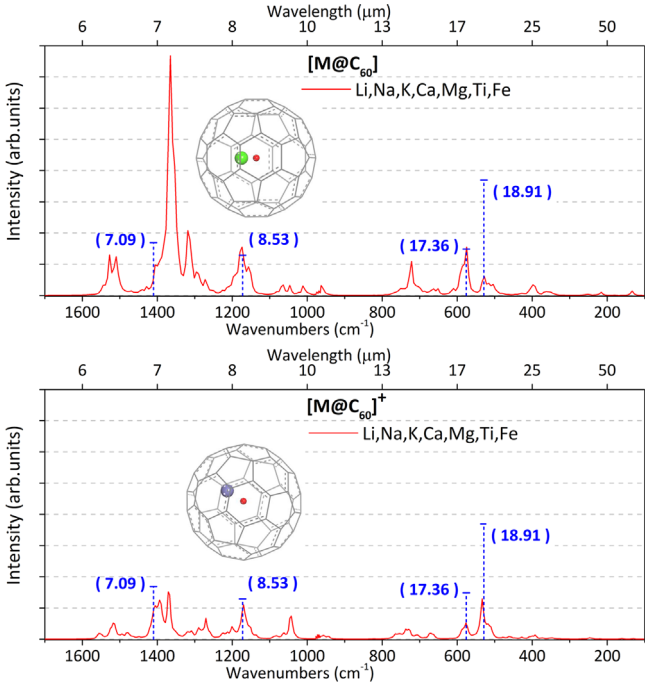

Figure 2. DFT simulated IR (∼5–50 μm) spectra of the mixture of metalloendofullerenes. Top panel: seven neutral [M@C_{60}]; bottom panel: seven charged $[M@C_{60}]^+$. The blue dashed lines are the same as in Figure 1. The insets display examples of the most common structures obtained but in this case a red dot depicts the centroid of the C_{60} carbon cage.

Multiple features appear in the 6–9 μm region, specially the highest intensity peak at 7.34 μm, which overcomes the 7.09 μm C_{60} feature. Similarly, above 14 μm, the spectral fingerprint of [M-C_{60}] is the emergence of several IR peaks accompanied with an inversion of the 17.4 μm/18.9 μm band ratio. The diversity of new 6–9 μm IR features in the [M-C_{60}] spectrum reflects the binding of the metal to the C_{60} carbon cage, while the change in the 17.4 μm/18.9 μm ratio (which are the vibrational modes related to the cage stretching) it is likely due to a charge redistribution also provoked by the metal. The C_{60} 17.4 μm/18.9 μm ratio displays values between 0.41 and 0.79, according to experiments and DFT calculations, respectively (Kern et al. 2013; Sadjadi et al. 2022); in our simulations such a ratio for C_{60} is 0.40 (see the blue dashed lines in Figure 1). However, the 17.4 μm/18.9 μm ratio in the [M-C_{60}] mixture spectrum is 1.89 (Figure 1). Interestingly, the 17.4 μm/18.9 μm ratio is not inverted (0.55) in the charged metalloexofullerene $[M\text{-}C_{60}]^+$ mixture spectrum (Figure 1), which is more characteristic of an electrostatic interaction (Jaeger et al. 2004; Szczepanski et al. 2006; Parker 2010) and noncovalent metal–C_{60} forces (Robledo et al. 2014), i.e., the lack of new IR features in the 6–9 μm C–C stretching region together with a global spectral resemblance to pristine C_{60}.

3.2. Endofullerenes

The neutral metalloendofullerenes [M@C_{60}] show their most intense feature at 7.32 μm because of the off-centered inclusion of the metal in the C_{60} cage (Figure 2). Such an effect creates a strong asymmetry in the C_{60} because carbon atoms trend to disrupt the cage in order to accommodate the metal. The perturbation of C–C stretching modes by the binding of the metal implies the whole cage instead of a section, like in the case of neutral metalloexofullerenes. This implies an important increment in the intensity of the IR features within the 6–9 μm region in comparison to pure C_{60} (Figure 2), even surpassing the intensity of the IR features for the neutral metalloexofullerenes mentioned above (Figure 1). The strong broadening and splitting of the [M@C_{60}] mixture spectrum in the 6–9 μm region is again an indication of the metal–carbon cage binding.[14] However, above 14 μm the spectral landscape of [M@C_{60}] considerably diminishes, specially the 18.9 μm feature intensity, which results in a 17.4 μm/18.9 μm ratio of 2.55. In the case of charged metalloendofullerenes $[M@C_{60}]^+$ the reduction of the intensity of the IR features takes place over the entire ∼5–50 μm spectral region, particularly, in the 6–9 μm C–C stretching region. Such intensity reduction likely implies a lack of charge transfer between the metal and C_{60} carbon cage. In spite of this, the 17.4 μm/18.9 μm ratio (0.40) is almost identical to the one for C_{60}.

3.3. Charge versus Neutrality

Both charged and neutral metallofullerenes would coexist in circumstellar envelopes since one of the reactants in the metallofullerenes formation, the metals, can be already ionized by the central star (e.g., García-Hernández et al. 2012). In any circumstellar environment, however, the metals have a particular abundance, implying that reliable IR spectra simulations should mix both neutral and charged species, including the specific metal abundances. For this, we have constructed the total weighted-mixture spectra in very different fullerene-rich circumstellar envelopes like those around PNe and RCB stars (for details see Appendix). Figures 3(a) and (b) show, respectively, the total and the total weighted-mixture spectra for the C_{60}–PNe case, where the intensity has been normalized for ease of comparison. We note that the formation probability of the endo- versus exofullerenes has not been considered because this would require the study of complex kinetic processes, which are out of the scope of this paper. We thus simply assume that both exo- and endofullerenes have the same formation probability.

The total mixture spectra has the neutral metallofullerenes as the dominant contributor with an integrated spectral area of 68% (see Figure 3(a)). Surprisingly, this drastically changes for the total weighted-mixture spectra (see Figure 3(b)), where the neutral metallofullerenes completely dominate the spectrum, with an integrated spectral area of 94%. The metal abundances and ionization fractions expected in C_{60}–PNe circumstellar environments are the two main factors producing such strong modifications in the total weighted-mixture spectra. This is because in C_{60}–PNe (i) the metal abundance follows the order of Mg > Fe ≫ Na > Ca > K ≃ Ti > Li (Karakas 2010; Karakas et al. 2018, see Appendix) and (ii) the most abundant metals (Fe, Mg) exhibit the lowest fractions of ionized atoms, around 5%–10%, even for the highest effective temperature, $T_{\rm eff} = 50{,}000$ K, observed in C_{60}–PNe (García-Hernández et al. 2012; Otsuka et al. 2014). Indeed, direct thermal effects over the IR intensity can be almost neglected; only very small deviations (a factor of 1.07; see the inset in Figure 3(b)) are predicted for the narrow $T_{\rm eff}$ range (∼25,000–50,000 K) of C_{60}–PNe. The noticeable modification

[14] Similarly to the neutral exofullerenes, the ∼7.0 μm feature (being not among the strongest features) is present but blended with other higher intensity features inside the 6–9 μm spectral region.

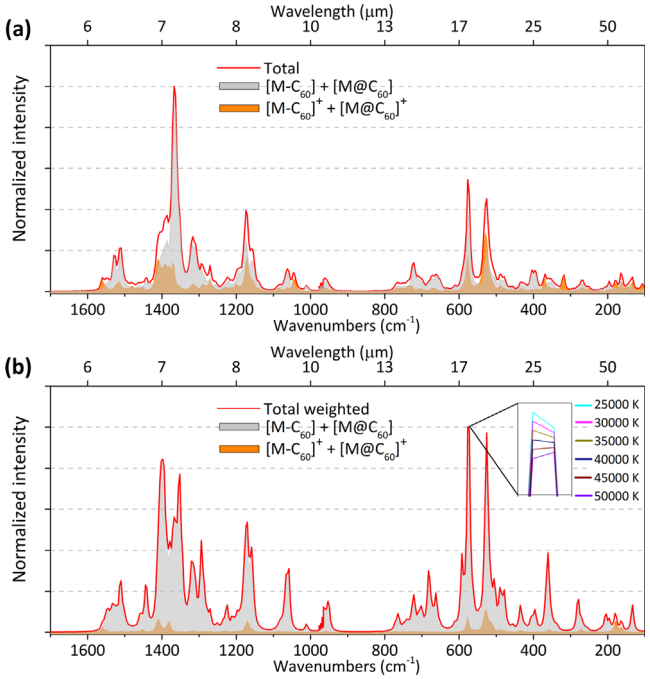

Figure 3. Contributions of neutral and charged metallofullerenes to (a) the total mixture spectrum from the 28 metallofullerenes and (b) the total weighted spectrum from abundances and the ion fraction. Neutral and charged species are denoted by the light gray and orange filled areas, respectively. An inset highlights the $T_{\rm eff}$-dependent change in the 17.4 μm feature intensity for the total weighted spectrum.

of the total weighted-mixture spectra prove the importance of the metal abundances and ionization fractions in order to obtain reliable IR-simulated spectra. The spectral landscape in Figure 3(b) is altered in such a way that the 17.4 μm/18.9 μm ratio varies from 1.21 to 1.03 (total versus total weighted spectra). Thus, our results indicate that the 17.4 μm/18.9 μm ratio can be used to track down the presence of charged versus neutral metallofullerenes.

Chemical stability is another key factor for the likely preponderance of neutral metallofullerenes. Table 1 displays the relative total energies ($E_{\rm tot}^{\rm rel}$; see also Section 2) of all metallofullerenes studied here. Energetically neutral metallofullerenes are the more stable species by an order of ~7 eV, which can be attributed to the interaction between the metal and C_{60}, where the charge is compensated. Oppositely, charged metallofullerenes create an uncompensated interaction with the C_{60} cage, specially for $[M@C_{60}]^+$ since the positive charge of the metal is embedded on the carbon cage, which requires more energy to stabilize this charge surrounded by an almost neutral environment. Furthermore, in some cases the C_{60} cage is slightly positively charged hindering the energetical stabilization even more.

Alternatively, once neutral metallofullerenes are formed, charged species can be generated via the photoionization reactions:

$$[M@C_{60}] \xrightarrow{h\nu} [M@C_{60}]^+$$
$$[M - C_{60}] \xrightarrow{h\nu} [M - C_{60}]^+.$$

Both reactions need to accomplish two requirements: (i) photons exciting the neutral metallofullerenes should have energies equal to the corresponding ionization potential and (ii) the production of charged metallofullerenes depends also on the amount of ionizing photons arriving. The first condition, the metallofullerenes ionization potential, can be inferred from the equation $IP = E_{\rm rel}^{\rm total}$charged $- E_{\rm rel}^{\rm total}$neutral using the values presented in Table 1 between analogous species (e.g., $[Ca@C_{60}]$ versus $[Ca@C_{60}]^+$). This gives a range from ~5 to 7 eV, which is an energy easily accessible for the photons emitted by the C_{60}–PNe central stars (CS; O- and B-type stars; Sternberg et al. 2003). The second condition depends on the flux of ionizing photons leaving the central star, but this flux decays when the central star is cooler (Sternberg et al. 2003). We thus estimate that for a $T_{\rm eff} = 40,000$ K PN central star, 50% of the ionizing photons would produce charged metallofullerenes, while for the cooler (<20,000 K) RCB stars the flux decays gradually to 10%. Such estimations allow us to observe the effect of the overproduction of charged metallofullerenes in the 17.4 μm/18.9 μm band ratio. Nevertheless, these are rough estimations since for the coolest RCB star V854 Cen ($T_{\rm eff} = 6750$ K) almost no ionizing photons are produced according to our blackbody models. Figure 4 displays the 17.4 μm/18.9 μm ratio as a function of the ionization level of neutral metallofullerenes. The data points associated with the curves of the RCB stars were calculated according to Appendix, using adequate abundances for these stars.

The negative slope observed for the three types of circumstellar envelopes indicate that the 17.4 μm/18.9 μm ratio decreases when more charged metallofullerenes are present, i.e., higher ionization level (Figure 4). The difference between the curves is a direct consequence of the metal abundances, which modify the initial amount of neutral metallofullerenes. Thus, the PNe curves cover a 17.4 μm/18.9 μm range of 0.73–1.23, while the RCB ranges are 1.14–1.88 (V854 Cen) and 1.12–1.97 (DY Cen). Thermal effects mainly imply an increment of the ionization level although we actually cannot discard possible temperature effects on the kinetics of metallofullerenes formation. Strictly, temperature effects could be important in the transformation of endo- to exofullerenes (or vice versa) but such study will be the subject of a future work. A simple approach to infer the endo/exoconcentration effect has been obtained from the total amount of neutral or charged species. Therefore, either exo- or endofullerene concentration has been doubled for both neutral or charged species. Figure 4 shows that an increment in the amount of endofullerenes (endo/exo 2:1) also produces an increment in the 17.4 μm/18.9 μm ratio with respect to the endo/exo 1:1 concentration, while an exofullerenes increment (endo/exo 1:2) reduces such intensity ratio. So, for the same ionization level, different 17.4 μm/18.9 μm ratios are obtained depending on the endo-/exoconcentration. This behavior stressed the marked loss of intensity in the 18.9 μm feature provoked by metalloendofullerenes. However, the general trend remains to be dominated by the presence of more neutral species against the charged ones. As the level of ionization rises we would expect that the curves corresponding to each circumstellar envelope tend to approximate each other.

4. Astrophysical Implications and Concluding Remarks

As it was mentioned above, Brieva et al. (2016) have highlighted that the use of C_{60} relative intrinsic strengths from laboratory data does not explain the large range of 17.4 μm/18.9 μm band ratios (~0.2–1.2) observed in the fullerene-rich circumstellar envelopes around PNe. One possible explanation is the presence of additional emitters contributing to the observed IR spectra. Fullerene-based molecules such as endo

Table 1
Total Relative Energies in eV (E_{tot}^{rel}) and the Charge on Metal (q^M) and the C_{60} Cage ($q^{C_{60}}$)

	[M@C_{60}]			[M-C_{60}]			[M@C_{60}]$^+$			[M-C_{60}]$^+$		
	E_{tot}^{rel}	q^M	$q^{C_{60}}$	E_{tot}^{rel}	q^M	$q^{C_{60}}$	E_{tot}^{rel}	q^M	$q^{C_{60}}$	E_{tot}^{rel}	q^M	$q^{C_{60}}$
Ca	0	+1.78	−1.78	0.22	+0.91	−0.91	5.54	+1.78	−0.78	5.23	+0.97	+0.03
Mg	0.34	+0.36	−0.36	0	+0.80	−0.80	6.06	+1.09	−0.09	5.34	+0.90	+0.10
Li	0	+0.91	−0.91	0.07	+0.91	−0.91	7.03	+0.91	+0.09	5.12	+0.93	+0.07
Na	0	+0.93	−0.93	0.21	+0.90	−0.90	5.37	+0.89	+0.11	5.04	+0.93	+0.07
K	0	+0.93	−0.93	0.56	+0.91	−0.91	5.36	+0.93	+0.07	5.16	+0.94	+0.06
Fe	1.41	+1.07	−1.07	0	+0.41	−0.41	6.89	+1.04	−0.04	5.61	+0.93	+0.07
Ti	0	+1.36	−1.36	0.46	+0.92	−0.92	5.88	+1.35	−0.35	5.89	+1.21	−0.21

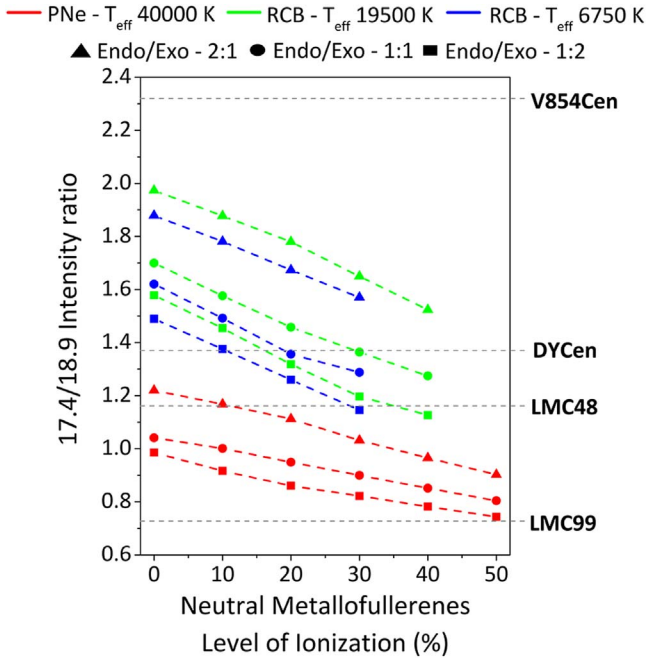

Figure 4. The 17.4 μm/18.9 μm ratio vs. the neutral metallofullerenes level of ionization. The several colors and symbols correspond to different circumstellar envelopes (PNe and RCB) and exo-/endofullerenes concentrations, respectively (see the legend). The horizontal dashed lines indicate the 17.4 μm/18.9 μm ratios observed in two C_{60}–PNe (LMC 48, LMC 99; García-Hernández et al. 2012), C_{60}–RCBs V854 Cen, and DY Cen (this work; García-Hernández et al. 2011).

(exo)hedral metallofullerenes and fullerene–PAH adducts, among others, are natural candidate species although, to our best knowledge, no additional emitter has been identified to date.

Our DFT calculations and corresponding simulated IR spectra for metallofullerene species reveal that the 17.4 μm/18.9 μm band ratio mainly depends on the metal abundances, ionization level, and endo/exoconcentration in the circumstellar envelopes. Interestingly, the theoretically predicted 17.4 μm/18.9 μm band ratios (∼0.7–1.2) for C_{60}–PNe agree reasonably well with those observed in Galactic and extragalactic C_{60}–PNe (∼0.2–1.2; Garcia-Hernandez et al. 2011b; Brieva et al. 2016); the match is quite exceptional for the Large Magellanic Cloud (LMC) PNe (∼0.7–1.1; Garcia-Hernandez et al. 2011b), which are the C_{60}–PNe with the metal abundances closest to the composition assumed in the construction of the total weighted-mixture metallofullerene spectra. The latter is exemplified in Figure 4 by the LMC PNe LMC 48 and LMC 99.

Furthermore, the consistency of our quantum-chemistry calculations goes beyond the C_{60}–PNe and also explains the astonishing anomalous 17.4 μm/18.9 μm ratios observed in the chemically peculiar RCB stars. The two known C_{60}–RCBs display a 18.9 μm feature much weaker than the 17.4 μm one (García-Hernández et al. 2011); 17.4 μm/18.9 μm ratios of ∼1.4 and 2.3 are observed in DY Cen and V854 Cen, respectively (Figure 4). The theoretically predicted 17.4 μm/18.9 μm band ratios (∼1.1–2.0) for the peculiar RCB compositions agree very well with the DY Cen observation, while V854 Cen displays a 17.4 μm/18.9 μm ratio larger than the predictions. This, however, is in agreement with the spectral analysis of their Spitzer spectra, which shows that the 17.4 μm feature is dominated by C_{60} emission in DY Cen, while such a feature in V854 Cen is a combination of C_{60} and PAH emission (García-Hernández et al. 2011). The unusually large 17.4 μm/18.9 μm ratios observed in the RCBs are naturally explained by a much larger contribution of neutral metallofullerenes, as expected from their lower T_{eff} and weaker UV radiation fields.

In short, we conclude that metallofullerenes are potential emitters contributing to the observed IR spectra in fullerene-rich circumstellar envelopes, providing for the first time an explanation for the fundamental problem of the large range of 17.4 μm/18.9 μm band ratios observed.

We emphasize that a perfect spectral match of the simulated metallofullerene IR spectra with the PNe and RCB Spitzer spectroscopic observations is not possible. Apart from the four strongest neutral C_{60} features, there is a no complete one-to-one correspondence and we cannot discard the presence of others carriers (even other fullerene-based species; see below) affecting the same IR features. However, from our quantum-chemistry calculations it seems clear that the neutral metallofullerenes species significantly contribute to the 6–9 μm C–C stretching region because of the metal–carbon cage binding effect (see Section 3). A similar spectral effect would be thus expected for other fullerene-based neutral species. Indeed, a genuine characteristic of fullerene-rich PNe environments with unusually high 17.4 μm/18.9 μm ratios like the LMC PNe analyzed here (see Figure 4) is the general presence of a broad and complex (with multiple components/peaks) IR feature at 6–9 μm (García-Hernández et al. 2012), something that strongly suggest the presence of fullerene-based neutral species such as neutral metallofullerenes, among others.

Finally, we note that most fullerene-rich circumstellar envelopes have been previously observed at low resolution ($R \sim 120$) by Spitzer, strongly limiting the detection of the weaker (and more specific) mid-IR features of endo(exo)hedral metallofullerenes (both neutral and charged; see Figures 1 to 3). Surprisingly, the only two C_{60}–MCPNe observed at higher

resolution ($R \sim 600$; $\sim$10–20 μm) with Spitzer display the presence of new IR emission features not previously observed in astrophysical environments (Garcia-Hernandez et al. 2011b). Such new IR emission features are potentially due to specific fullerene-based species such as metallofullerenes; most of them, however, remained as tentative because of the low-quality (signal-to-noise ratio (S/N) $\sim$ 10 at the continuum) Spitzer spectra (Garcia-Hernandez et al. 2011b). The JWST, with a much higher sensitivity (and spectral resolution) than Spitzer, has the potential to unambiguously detect the spectral signatures of new IR emission features potentially due to metallofullerenes (or even other fullerene-based species). Thus, high S/N (>100) and high-resolution ($R \sim 2400$ on average) JWST spectroscopic observations of fullerene-rich envelopes (e.g., C_{60} PNe and RCBs) are strongly encouraged in order to confirm or refute the presence of metallofullerenes in circumstellar environments.

We acknowledge support from the ACIISI, Gobierno de Canarias, and the European Regional Development Fund (ERDF) under a grant with the reference PROID2020010051 as well as the State Research Agency (AEI) of the Spanish Ministry of Science and Innovation (MICINN) under grants PID2020-115758GB-I00 and PID2019-110091GB-I00. This article is based upon work from European Cooperation in Science and Technology (COST) Action NanoSpace, CA21126, supported by COST.

Appendix
Weighted Simulated Spectra

The IR intensity (I) can be defined as $I \propto (\partial\mu/\partial x)^2$ where $\partial\mu$ stands for the change in the dipole moment and ∂x is the displacement produced by the corresponding vibrational mode. Another factor that determines the peak intensity in the IR is the concentration (n_i) of i molecules or species:

$$I \propto \sum_{i}^{j} \left(\frac{\partial\mu}{\partial x}\right)^2 n_i. \tag{A1}$$

The summation indicates the contribution from species ith to jth. In our case these species are the metallofullerenes obtained in the reactions between the metal (M) and C_{60}:

$$\begin{aligned} \mathrm{M} \; + \; \mathrm{C_{60}} &\rightarrow [\mathrm{M@C_{60}}] \text{ or } [\mathrm{M} - \mathrm{C_{60}}] \\ \mathrm{M^+} + \mathrm{C_{60}} &\rightarrow [\mathrm{M@C_{60}}]^+ \text{ or } [\mathrm{M} - \mathrm{C_{60}}]^+ \\ \mathrm{M} \; + \; \mathrm{C_{60}^+} &\rightarrow [\mathrm{M@C_{60}}]^+ \text{ or } [\mathrm{M} - \mathrm{C_{60}}]^+. \end{aligned}$$

We note that the third reaction implying a metal and C_{60}^+ can be discarded because there is no evidence for the presence of C_{60}^+ in the circumstellar environments around PNe and RCB stars (Berné et al. 2013; Cordiner et al. 2019). According to the aforementioned reactions, the metallofullerene concentration thus depends on the amount of M, M^+, and C_{60}. From stellar nucleosynthesis models or direct measurements (see below) it is possible also to extract the total metal abundances $M_T = M + M^+$, while C_{60} can be estimated as the excess reactant due to the larger abundance of carbon $C >>> M_T$. Fullerene-rich PNe display a narrow $T_{\rm eff}$ range ($\sim$30,000–50,000 K) and chemical abundances similar to their progenitors, i.e., slightly metal-poor ($Z \sim 0.004$) and low-mass (1.5–2.5 $M_\odot$) asymptotic giant branch (AGB) stars (Otsuka et al. 2014). We note that our simulated IR spectra do not change significantly for 1.5–2.5 $M_\odot$, due to the fact that the relative metal abundances remain almost constant in this mass range. Thus, for C_{60}–PNe the metal abundances for a 2 $M_\odot$ AGB star were taken from AGB nucleosynthesis models (Karakas 2010; Karakas et al. 2018); note also that not all metals considered here have been directly measured in C_{60}–PNe and we thus need the metal abundance values from theoretical predictions. However, the total metal abundance measurements reported by Jeffery et al. (2011) were used for the only two fullerene-rich RCBs, V854 Cen ($T_{\rm eff} = 6750$ K) and DY Cen ($T_{\rm eff} = 19{,}500$ K; García-Hernández et al. 2011). Accordingly, M and M^+ are the limiting factors in the metallofullerenes formation. Using the well-known Saha equation (Saha 1920) we are able to predict the concentration of M and M^+ by

$$\frac{n_{M^+}^2}{n_M} = \frac{G_{M^+} g_e}{G_M} \frac{(2\pi m_e kT)^{3/2}}{h^3} \exp\left(-\frac{IP_1}{kT_{\rm eff}}\right), \tag{A2}$$

with n_{M^+} and n_M being the density of the atoms in ionized and neutral states, respectively. The degeneracy of the ionized or neutral state is represented by G_{M^+} or G_M while g_e is the electron degeneracy. Finally, $T_{\rm eff}$ is the effective temperature of the PNe/RCB central star, and IP_1 denotes the first ionization potential of the metal; the remaining variables are the Boltzmann (k), Planck (h), and the electron mass m_e constants. Applying also $n_{M_T} = n_{M^+} + n_M$ and $\chi = \frac{n_{M^+}}{n_{M_T}}$, where χ indicates the fraction of ionized atoms, we obtain

$$\frac{\chi^2}{1-\chi} = \frac{\frac{G_{M^+} g_e}{G_M} \frac{(2\pi m_e kT)^{3/2}}{h^3} \exp\left(-\frac{IP_1}{kT_{\rm eff}}\right)}{n_{M_T}}. \tag{A3}$$

From Equation (A3) we extract n_{M^+} and n_M to weigh the intensities according to

$$I_{M^+} \propto \sum_{i}^{j} \left(\frac{\partial\mu}{\partial x}\right)^2 n_{M^+}, \tag{A4}$$

$$I_M \propto \sum_{i}^{j} \left(\frac{\partial\mu}{\partial x}\right)^2 n_M, \tag{A5}$$

$$I_T = I_M + I_{M^+}. \tag{A6}$$

The variable I_T is used to construct the total weighted-mixture spectra of metallofullerenes and I_M,I_{M^+}, the corresponding neutral and charged contributions.

ORCID iDs

R. Barzaga https://orcid.org/0000-0002-9827-2762
D. A. García-Hernández https://orcid.org/0000-0002-1693-2721
S. Díaz-Tendero https://orcid.org/0000-0001-6253-6343
SeyedAbdolreza Sadjadi https://orcid.org/0000-0003-3529-0178
A. Manchado https://orcid.org/0000-0002-3011-686X
M. Alcami https://orcid.org/0000-0002-3753-5215

References

Bader, R. 1990, Atoms in Molecules: A Quantum Theory (Oxford Univ. Press: Oxford)
Becke, A. D. 1993, JChPh, 98, 5648
Berné, O., Mulas, G., & Joblin, C. 2013, A&A, 550, L4

Brieva, A. C., Gredel, R., Jager, C., Huisken, F., & Henning, T. 2016, ApJ, 826, 122
Cami, J., Bernard-Salas, J., Peeters, E., & Malek, S. E. 2010, Sci, 329, 1180
Campbell, E. K., Holz, M., Gerlich, D., & Maier, J. P. 2015, Natur, 523, 322
Cordiner, M. A., Linnartz, H., Cox, N. L. J., et al. 2019, ApJL, 875, L28
Dennington, R., Keith, T. A., & Millam, J. M. 2019, GaussView Version 6, https://gaussian.com/gaussview6/
Ditchfield, R., Hehre, W. J., & Pople, J. A. 1971, JChPh, 54, 724
Dunk, P. W., Adjizian, J.-J., Kaiser, N. K., et al. 2013, PNAS, 110, 18081
Frisch, M. J., Trucks, G. W., Schlegel, H. B., et al. 2016, Gaussian 16 Revision C.01, https://gaussian.com
Garcia-Hernandez, D. A., Cataldo, F., & Manchado, A. 2013, MNRAS, 434, 415
Garcia-Hernandez, D. A., Iglesias-Groth, S., Acosta-Pulido, J. A., et al. 2011b, ApJL, 737, L30
García-Hernández, D. A., Kameswara Rao, N., & Lambert, D. L. 2011, ApJ, 729, 126
García-Hernández, D. A., Manchado, A., Garcia-Lario, P., et al. 2010, ApJL, 724, L39
García-Hernández, D. A., Villaver, E., García-Lario, P., et al. 2012, ApJ, 760, 107
Jaeger, T. D., van Heijnsbergen, D., Klippenstein, S. J., et al. 2004, JAChS, 126, 10981
Jeffery, C. S., Karakas, A. I., & Saio, H. 2011, MNRAS, 414, 3599
Karakas, A. I. 2010, MNRAS, 403, 1413
Karakas, A. I., Lugaro, M., Carlos, M., et al. 2018, MNRAS, 477, 421
Keith, T. A. 2019, AIMAll (Version 19.10.12), http://aim.tkgristmill.com/
Kern, B., Strelnikov, D., Weis, P., Bottcher, A., & Kappes, M. M. 2013, JPCA, 117, 8251
Kwok, S. 2016, A&ARv, 24, 8
Lee, C., Yang, W., & Parr, R. G. 1988, PhRvB, 37, 785
Otsuka, M., Kemper, F., Cami, J., Peeters, E., & Bernard-Salas, J. 2014, MNRAS, 437, 2577
Parker, S. F. 2010, JPCA, 114, 1657
Robledo, M., Aguirre, N. F., Diaz-Tendero, S., Martin, F., & Alcami, M. 2014, RSCAd, 4, 53010
Sadjadi, S., Parker, Q. A., Hsia, C.-H., & Zhang, Y. 2022, ApJ, 934, 75
Saha, M. N. 1920, Lond. Edinb. Dublin Philos. Mag. J. Sci., 40, 472
Sternberg, A., Hoffmann, T. L., & Pauldrach, A. W. 2003, ApJ, 599, 1333
Szczepanski, J., Wang, H., Vala, M., et al. 2006, ApJ, 646, 666
Wang, Y., Díaz-Tendero, S., Alcamí, M., & Martín, F. 2017, JAChS, 139, 1609
Zapata Trujillo, J. C., & McKemmish, L. K. 2022, WIREs Comput. Mol. Sci., 12, e1584